Geophysical Research Letters

Supporting Information for

Numerical Investigation of Multiphase Flow through Complex Fractures

Prakash Purswani[1,*], Javier E. Santos[1], Jeffrey D. Hyman[1], Eric J. Guiltinan[1]

[1]Earth and Environmental Sciences Division, Los Alamos National Laboratory, Los Alamos, NM, 87545

*Corresponding author at ppurswani@lanl.gov, Ph. (832)-7015366

Contents of this file

Text S1

Figure S1 shows the simulation time for the cases discussed in Figure 1d of the main manuscript. These were carried out on the LANL's Chicoma Nvidia A100 GPU cluster using one node and four GPUs. A linear relationship is observed on the log-log scale between the simulation time and capillary number set for the simulation. The simulations were terminated at the breakthrough saturation. Among the various fracture and flow parameters tested, capillary number (flow velocity) was the dominant parameter that controlled the simulation time with the maximum time of ~1000mins for the lowest capillary number ($5x10^{-6}$) tested.

Figure S2 compares the displacement profiles as discussed in Figure 2a of the main manuscript. Here, we compare similar breakthrough saturations for different capillary numbers and viscosity ratio in a single rough fracture. We find that despite similar breakthrough saturation of ~0.7, the way the fluid invasion occurs is quite different. A

combination of high capillary number and high viscosity ratio or low capillary number and low viscosity ratio leads to achieving these similar breakthrough saturations. In addition, Figures S2 b to e show the normalized front migration against the saturation for the viscosity ratios of 10, 1.0, 0.1, 0.02, respectively.

Figure S3 shows the data points for the different simulations used to construct Figure 4 of the main manuscript.

Figure S4 shows the mean and standard deviation of each subplot inside Figure S3. From this Figure, we can visualize that breakthrough saturations are delayed for lower rms roughness. The impact of contact angle is found to be less relevant for rms roughness of 2. For contact angle, higher contact angles show higher breakthrough saturations, showing gradual advance of the invading phase. We provide the linear fit equation and best fit measures for the fits shown in Figure S4 c and d as follows,

for $\theta = 30°$, BTS = -0.0925R + 1.0684 (R^2 = 0.9667),
for $\theta = 50°$, BTS = -0.0888R + 1.1122 (R^2 = 0.9966), and
for $\theta = 70°$, BTS = -0.0721R + 1.1026 (R^2 = 0.9674).
For R = 2, BTS = 0.001θ + 0.8748 (R^2 = 0.9757)
for R = 4, BTS = 0.0047θ + 0.5245 (R^2 = 0.9887), and
for R = 6, BTS = 0.0031θ + 0.4345 (R^2 = 0.9637).

Here, BTS is the breakthrough saturation, θ is the contact angle, and R is the rms roughness value.

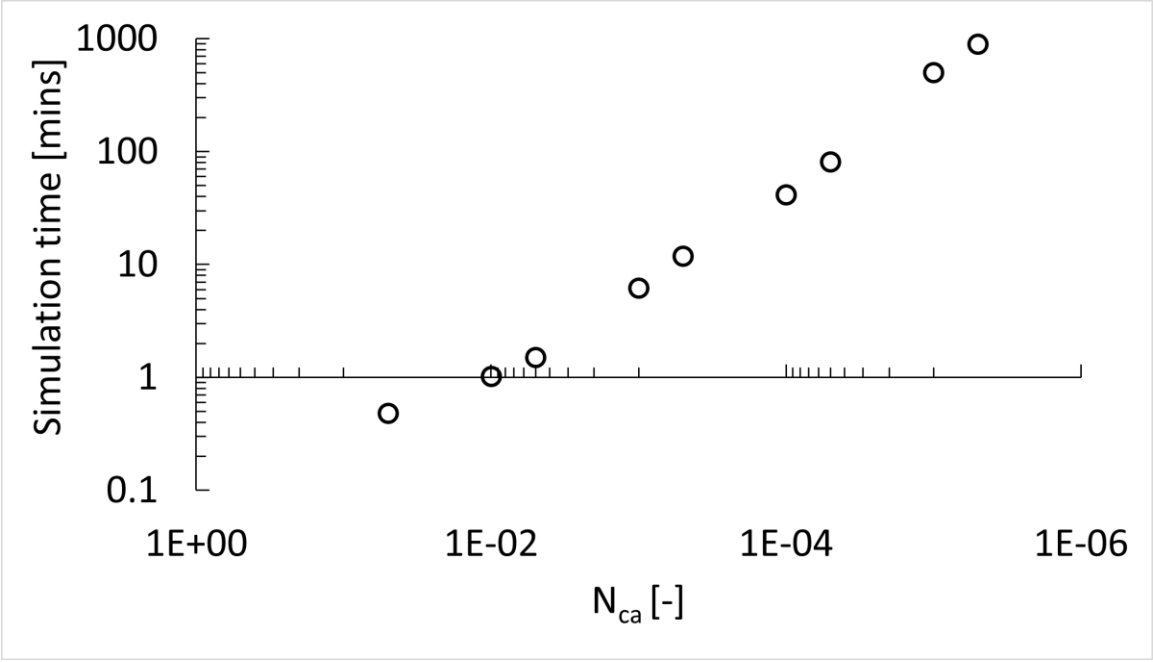

Figure S1. Simulation time for a set of cases. The cases shown here are discussed in Figure 1d of the main manuscript.

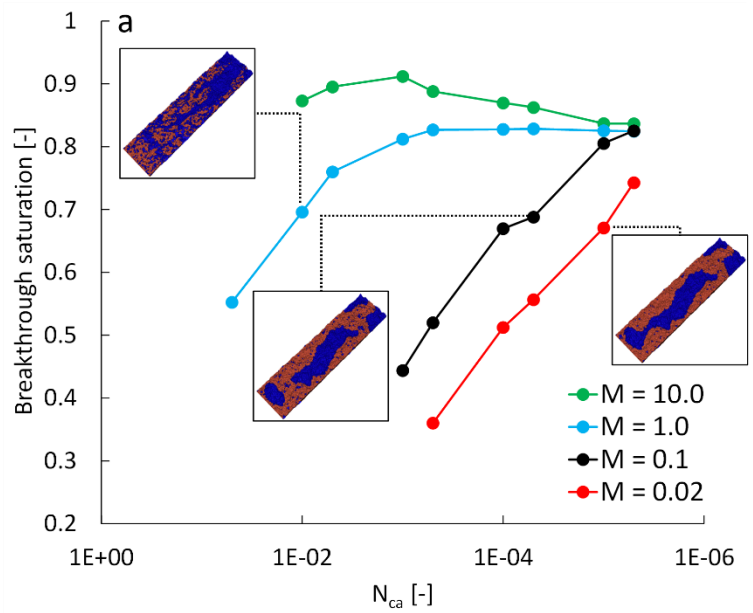
a
Breakthrough saturation [-]
1
0.9
0.8
0.7
0.6
0.5
0.4
0.3
0.2
1E+00
1E-02
1E-04
1E-06
N_{ca} [-]
M = 10.0
M = 1.0
M = 0.1
M = 0.02

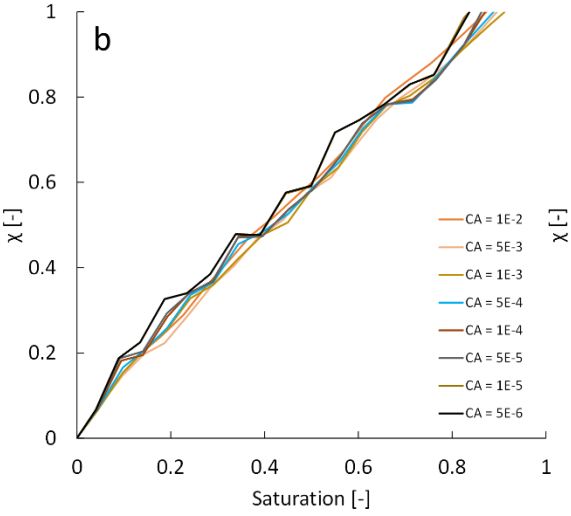
b
χ [-]
Saturation [-]
CA = 1E-2
CA = 5E-3
CA = 1E-3
CA = 5E-4
CA = 1E-4
CA = 5E-5
CA = 1E-5
CA = 5E-6

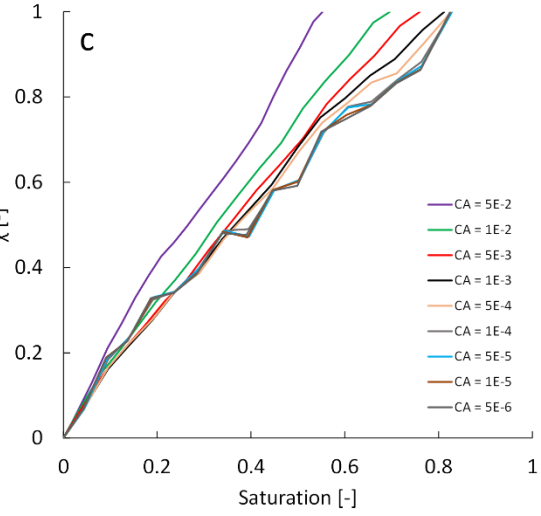
c
χ [-]
Saturation [-]
CA = 5E-2
CA = 1E-2
CA = 5E-3
CA = 1E-3
CA = 5E-4
CA = 1E-4
CA = 5E-5
CA = 1E-5
CA = 5E-6

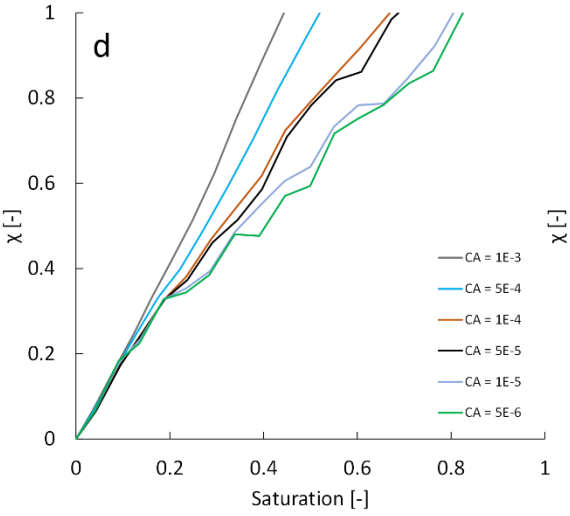
d
χ [-]
Saturation [-]
CA = 1E-3
CA = 5E-4
CA = 1E-4
CA = 5E-5
CA = 1E-5
CA = 5E-6

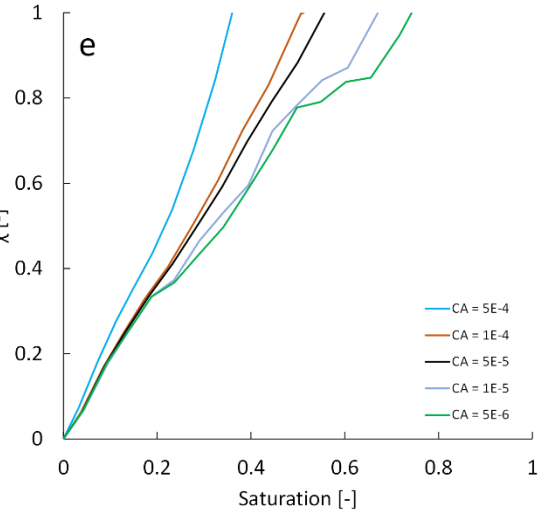
e
χ [-]
Saturation [-]
CA = 5E-4
CA = 1E-4
CA = 5E-5
CA = 1E-5
CA = 5E-6

Figure S2. Comparing breakthrough saturation for different capillary numbers and viscosity ratios in a single complex fracture (same as Figure 2a of the main manuscript) to compare fluid migration profiles for approximately the same breakthrough saturations across different capillary number and viscosity ratios. (b), (c), (d), and (e) are the invading front profiles for the four viscosity ratios, 10.0, 1.0, 0.1, and 0.02, respectively. Here all plots correspond to seed one. The different viscosity ratios during the simulations were achieved by varying the invading and receding phase viscosities (Table 1 in main manuscript). The range of capillary numbers investigated was calibrated for each viscosity ratio considering that very high or low values of capillary numbers caused numerical instability during the simulations.

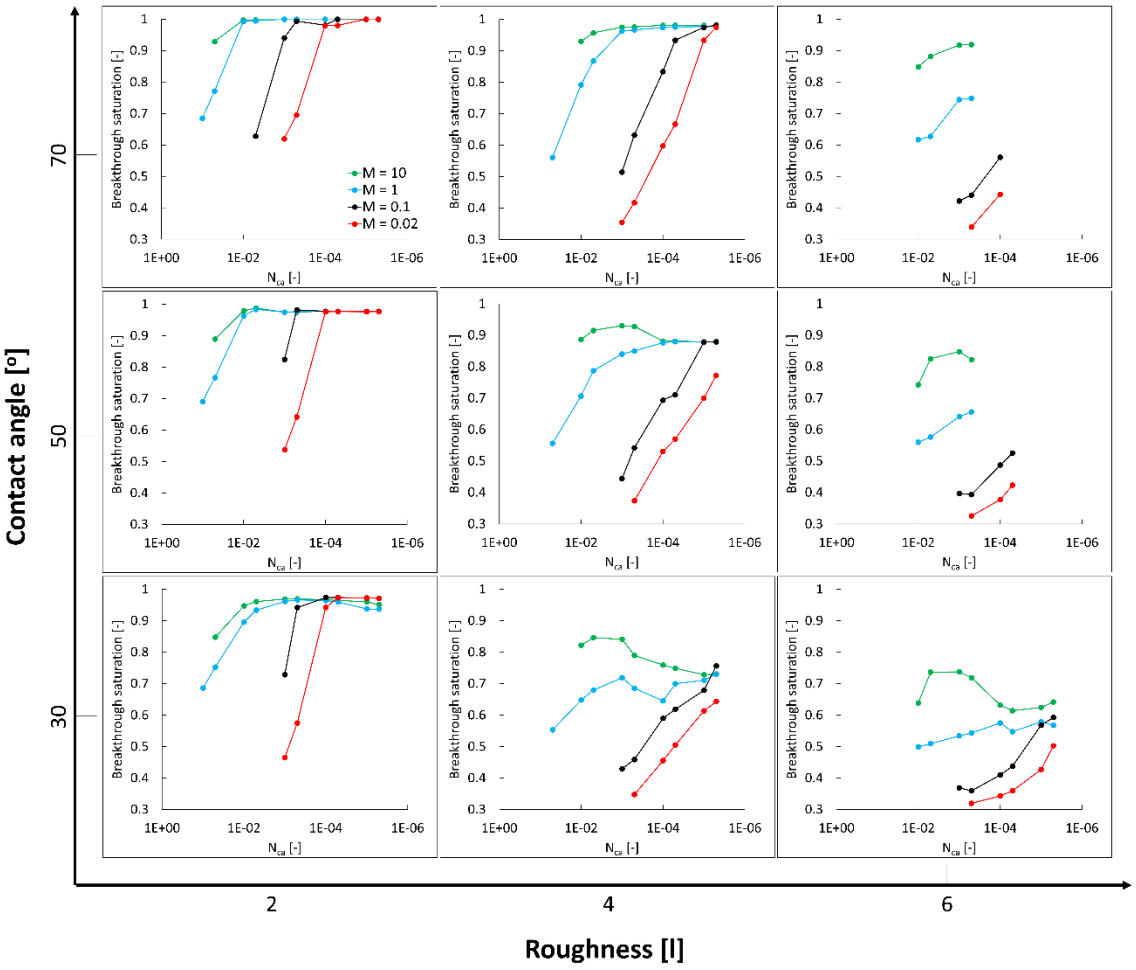

Figure S3. Simulation data used for the development of displacement pattern phase diagrams discussed in Figure 3 of the main manuscript. Three different rms roughness values (2, 4, and 6) and three different contact angle cases (30°, 50°, and 70° are considered for the full range of capillary numbers and viscosity ratios discussed in Figure 3 of the main

manuscript. All simulations discussed here are for seed one and the Hurst exponent was fixed at 0.7.

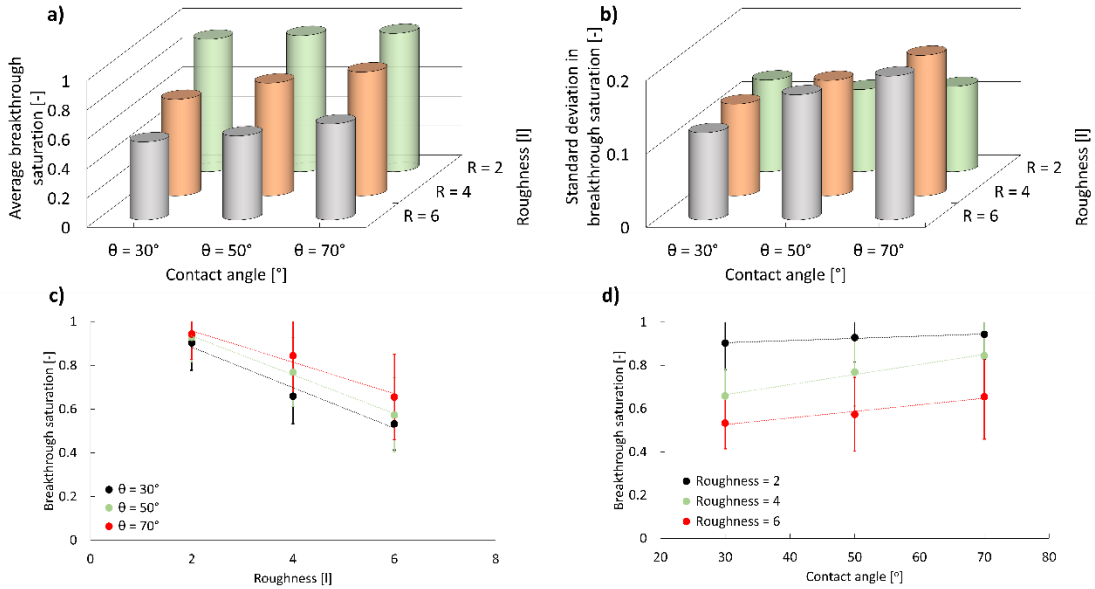

Figure S4. Average breakthrough saturation and (b) standard deviation for the data discussed in Figure S3. (c) Mean saturation plotted for different contact angles and (d) roughness values.

Rms roughness [l]	Estimated variance [l^2]	Standard deviation [l]	Mean aperture [l]	λ [-]
2	6.59	2.57	15	0.17
4	26.40	5.14	15	0.34
6	58.00	7.62	15	0.51

Table S1. Estimated dimensionless roughness parameter. Definition from Hu et al. (2019) and Lan et al. (2020). The correlation lengths for the surfaces were 26mm to 47mm in the X and Y directions, respectively.

References:

Hu, R., Zhou, C.-X., Wu, D.-S., Yang, Z. & Chen, Y.-F. (2019), 'Roughness control on multiphase flow in rock fractures', Geophysical Research Letters 46(21), 12002–12011.416 URL: https://agupubs.onlinelibrary.wiley.com/doi/abs/10.1029/2019GL084762

Lan, T., Hu, R., Yang, Z., Wu, D.-S. & Chen, Y.-F. (2020), 'Transitions of fluid invasion patterns in porous media', Geophysical Research Letters 47(20), e2020GL089682. e2020GL089682 2020GL089682. URL: https://agupubs.onlinelibrary.wiley.com/doi/abs/10.1029/2020GL089682